Defects and transport in $Pr_xCe_{1-x}O_{2-\delta}$: Composition trends

Sean R. Bishop[a)]
Department of Materials Science and Engineering, Massachusetts Institute of Technology, Cambridge, Massachusetts 02139; and International Institute for Carbon Neutral Energy Research (WPI-I2CNER), Kyushu University, Nishi-ku Fukuoka, 819-0395, Japan

Todd S. Stefanik[b)] and Harry L. Tuller[c)]
Department of Materials Science and Engineering, Massachusetts Institute of Technology, Cambridge, Massachusetts 02139

(Received 12 February 2012; accepted 26 March 2012)

Nonstoichiometric mixed ionic and electronic conductors (MIECs) find use as oxygen permeation membranes, cathodes in solid oxide fuel cells, oxygen storage materials in three-way catalysts, and chemoresistive gas sensors. Praseodymium–cerium oxide ($Pr_xCe_{1-x}O_{2-\delta}$) solid solutions exhibit MIEC behavior in a relatively high and readily accessible oxygen partial pressure (P_{O_2}) regime and as such serve as model systems for investigating the correlation between thermodynamic and kinetic properties as well as exhibiting high performance figures of merit in the above applications. In this paper, we extend recently published results for $Pr_{0.1}Ce_{0.9}O_{2-\delta}$ to include values of $x = 0$, 0.002, 0.008, 0.1, and 0.20 (in $Pr_xCe_{1-x}O_{2-\delta}$) to test how both defect and transport parameters depend on Pr fraction. Important observed trends with increasing x include increases in oxygen ion migration energy and MIEC and reductions in vacancy formation and Pr ionization energies. The implications these changes have for potential applications of $Pr_xCe_{1-x}O_{2-\delta}$ are discussed.

I. INTRODUCTION

Nonstoichiometric oxides with either the fluorite or perovskite structure are of great interest in energy conversion, automotive emissions control, and gas sensing applications given their ability to support high levels of oxygen ion and/or electronic transport with consequent ready exchange of oxygen with the gas phase. As such, they find use as oxygen permeation membranes, electrodes in solid oxide fuel cells (SOFCs), oxygen storage materials in three-way catalysts, and chemoresistive gas sensors. Fluorite-structured ceria (CeO_2) readily forms highly oxygen-deficient solid solutions with lower valent cations such as Gd, Sm, and Y and exhibits some of the highest recorded oxygen ion conductivities at elevated temperatures. This renders it of great interest as a solid electrolyte in intermediate temperature SOFCs.[1,2] Under reducing conditions, at elevated temperatures, Ce begins to reduce to the 3+ valence state, resulting in the introduction of both vacancies and quasi-free electrons, leading to mixed ionic and electronic conductivity (MIEC) and the degradation of its electrolytic properties.[3,4] On the other hand, MIEC materials can be advantageous, e.g., as electrodes in SOFCs since they render the entire electrode surface active for the reduction or oxidation of oxygen, as opposed to being limited to the triple-phase boundaries.[5] Furthermore, oxygen separation membranes utilizing MIECs allow for single-phase materials to simultaneously provide both oxygen diffusion and the necessary counterflow of electrons. The introduction of more easily reduced cations such as Pr or Tb into ceria allows the material to begin to reduce even under oxidizing conditions.[6,7]

In recent publications, the authors of this work reported in detail on the defect,[7–9] transport,[7,9,10] optical,[11] and mechanical[12–14] properties of $Pr_xCe_{1-x}O_{2-\delta}$ (PCO) with $x = 0.1$. Some of the important features of $Pr_{0.1}Ce_{0.9}O_{2-\delta}$ include the introduction of MIEC behavior under oxidizing conditions; sample coloration, connected with the formation of a Pr-based impurity band; as well as chemical expansion accompanied by a decrease in the energy needed to form oxygen vacancies with reduction. In this paper, we examine a range of compositions in the PCO system from $x = 0.002$ to 0.20 to understand how both defect and transport parameters depend on x. Important observed trends with increasing x include increases in oxygen ion migration energy and MIEC and reductions in vacancy formation and Pr ionization energies. The implications these changes have for potential applications of $Pr_xCe_{1-x}O_{2-\delta}$ are discussed.

II. THEORY

The key defect reactions describing the reduction of ceria, electron–hole generation, oxygen anti-Frenkel disorder,

[a)]Address all correspondence to this author.
e-mail: bishop@i2cner.kyushu-u.ac.jp
[b)]Present address: Nanocerox, Inc., Ann Arbor, MI 48108
[c)]This author was an editor of this focus issue during the review and decision stage. For the *JMR* policy on review and publication of manuscripts authored by editors, please refer to http://www.mrs.org/jmr-editor-manuscripts/
DOI: 10.1557/jmr.2012.130

 © Materials Research Society 2012

https://doi.org/10.1557/jmr.2012.130 Published online by Cambridge University Press

and Pr reduction are summarized, using Kröger–Vink notation, in Table I (see also Ref. 8). In each case, the defect reaction and the corresponding mass action equation is provided in terms of the corresponding equilibrium constants $K_i(T) = K_i^0 \exp(-H_i/kT)$, where T, k, and H_i are the absolute temperature, Boltzmann constant, and enthalpy of the reaction i, respectively. It should be noted that Eq. (5) is simply the product of Eq. (1) and the square of Eq. (4) and thus, $H_{r,\mathrm{Pr}} = H_r + 2H_{\mathrm{Pr}}$. The effective reduction enthalpy, $H_{r,\mathrm{Pr}}$, is thus reduced (H_{Pr} is negative) from that of undoped ceria, H_r, by twice the ionization energy of Pr, $2H_{\mathrm{Pr}}$.

In the charge neutrality relation [Eq. (6); Table I], it is assumed that p and oxygen interstitial concentration, $[O_i^{//}]$, are negligible given that PCO is assumed to be oxygen deficient at all accessible experimental conditions. The mass and site conservation relationships, on a molar basis, are given by Eqs. (7) and (8) in Table I, respectively. Equations (1)–(8) were rearranged and numerically solved for the concentrations of all listed species.

Given the large changes in stoichiometry that can be induced in the ceria system upon reduction, it would come as no surprise to find that the enthalpy of reduction of both undoped and Pr-doped ceria would vary with nonstoichiometry. This was indeed found previously for $Pr_{0.1}Ce_{0.9}O_{2-\delta}$ with the enthalpy following a linear dependence of the form.[9]

$$H_r = H_r^{\mathrm{o}} + f\delta \quad , \tag{9}$$

where H_r^{o} is the enthalpy of reduction when the oxygen vacancy concentration is zero (i.e., in $Pr_xCe_{1-x}O_{2-\delta}$) and f is the linear coefficient.

The total electrical conductivity of a solid is given as the sum of all species that contribute to conduction through the following equation.

$$\sigma_{\mathrm{total}} = \sum_i |Z_i| e [i] u_i \quad , \tag{10}$$

where z_i, e, and μ_i are the ith specie's charge, charge of an electron, and mobility, respectively. The mobility of an ion or a small polaron in the dilute concentration is defined as,[4]

$$\mu_i = \frac{\mu_i^{\circ}}{T} \exp\left(-\frac{H_{m,i}}{kT}\right) \quad , \tag{11}$$

where μ_i is the mobility preexponential and $H_{m,i}$ is the enthalpy of migration for the charge carrier. Equation (11) is used for both oxygen vacancies and electrons in the ceria conduction band. The small polaron model requires hopping of an electron from a Pr^{3+} to a Pr^{4+}, meaning that when the concentration of Pr^{3+} is high and Pr^{4+} is low, there is a low probability of an available site to jump into and so mobility decreases. This type of conduction is described by the following equation for PCO with $x = 0.1$ and 0.2.[4]

$$\mu_{\mathrm{Pr}} = \frac{\mu_{\mathrm{Pr}}^{\circ}\left(x - \left[\mathrm{Pr}_{\mathrm{Ce}}^{/}\right]\right)}{T} \exp\left(-\frac{H_{m,\mathrm{Pr}}}{kT}\right) \quad . \tag{12}$$

For small polaron conduction within the ceria conduction band, $[Ce_{Ce}^{/}]$ is assumed to remain dilute so that all neighboring Ce sites can be assumed to be available for a jump. Thus, for electron hopping in the ceria conduction band, Eq. (11) can be used instead.

III. EXPERIMENTAL METHODS

$Pr_xCe_{1-x}O_{2-\delta}$ sample preparation and measurement is discussed in detail previously[7,15] with a brief description given here. Powders were prepared for values of $x = 0$,

TABLE I. Key defect reactions and associated mass action relations are listed in Eqs. (1)–(5), the approximated charge neutrality relationship is Eq. (6), the Pr mass conservation relationship is Eq. (7), and the oxygen site conservation relationship is Eq. (8).

Defect reaction	Mass action relation	Equation number
$O_O^{\times} \leftrightarrow V_O^{\bullet\bullet} + 2e^{/} + 1/2O_2(g)$	$\frac{[V_O^{\bullet\bullet}]n^2 P_{O_2}^{1/2}}{[O_O^{\times}]} = K_r^{\circ}\exp\left(-\frac{H_r}{kT}\right)$	(1)
$\mathrm{nil} \leftrightarrow e^{/} + h^{\bullet}$	$np = N_C N_V \exp(-E_g/kT)$	(2)
$O_O^{\times} \leftrightarrow O_i^{//} + V_O^{\bullet\bullet}$	$\frac{[O_i^{//}][V_O^{\bullet\bullet}]}{[O_O^{\times}]} = K_F^{\circ}\exp\left(-\frac{H_F}{kT}\right)$	(3)
$Pr_{Ce}^{\times} + e^{/} \leftrightarrow Pr_{Ce}^{/}$	$\frac{[Pr_{Ce}^{/}]}{[Pr_{Ce}^{\times}]n} = K_{\mathrm{Pr}}^{\circ}\exp\left(-\frac{H_{\mathrm{Pr}}}{kT}\right)$	(4)
$2\,Pr_{Ce}^{\times} + O_O^{\times} \leftrightarrow 2\,Pr_{Ce}^{/} + V_O^{\bullet\bullet} + 1/2O_2(g)$	$\frac{[Pr_{Ce}^{/}]^2[V_O^{\bullet\bullet}]P_{O_2}^{1/2}}{[Pr_{Ce}^{\times}]^2[O_O^{\times}]} = K_{r,\mathrm{Pr}}^{\circ}\exp\left(-\frac{H_{r,\mathrm{Pr}}}{kT}\right)$	(5)
$\left[Pr_{Ce}^{/}\right] + n = 2\left[V_O^{\bullet\bullet}\right]$	...	(6)
$\left[Pr_{Ce}^{/}\right] + \left[Pr_{Ce}^{\times}\right] = x$	...	(7)
$\left[O_O^{\times}\right] + \left[V_O^{\bullet\bullet}\right] = 2$	...	(8)

https://doi.org/10.1557/jmr.2012.130 Published online by Cambridge University Press

0.002, 0.008, 0.1, and 0.20 by oxalate coprecipitation (OP).[16] In OP, a 1 M solution of metal nitrates was dripped into 0.5 M oxalic acid with complete precipitation of the metals, followed by filtering, drying, and calcination at 700 °C for at least an hour to form PCO. The powders were pressed to yield either cylindrical or bar pellets and sintered at >1400 °C.

Samples were cut into bars approximately 3 × 3 × 10 mm for four-point DC conductivity measurements. Pt wires were wrapped around the bar at four different positions and Pt paste (Englehard #6082, Iselin, NJ) was applied to make good connections between each wire and the bar. A Nernst-type zirconia oxygen sensor monitored the P_{O_2}, controlled either by mixtures of inert gas and oxygen, a homemade oxygen pump, or controlled mixtures of CO and CO_2. The error in conductivity measurements was estimated to be 7% of each measured value.

Wave length dispersive spectroscopy was performed to determine the Pr concentration using a JEOL electron microprobe (JXA-733 Superprobe) with metal phosphate standards before measurement. Phase purity was confirmed using x-ray diffraction on a Rigaku powder diffractometer (Rigaku Corporation, Tokyo, Japan).

Defect and conductivity modeling was performed using Matlab (Mathworks, Natick, MA). Unless otherwise stated, parameters in the models were determined using the Gauss–Newton method of nonlinear regression with partial derivatives approximated numerically (see, e.g., Ref. 7). Initial estimations were refined visually and then, regression was performed in a stepwise iterative manner, with a maximum of two parameters being determined at a time to avoid instabilities in the program. Error estimates for modeled parameters are reported for an approximate 95% confidence interval of the regressed model.

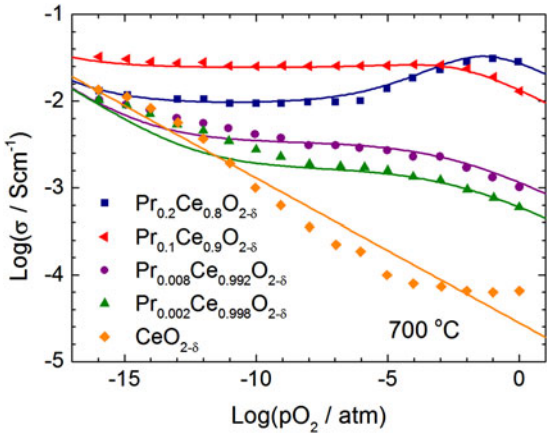


FIG. 1. Log s versus log P_{O_2} for a series of compositions in the system $Pr_xCe_{1-x}O_{2-\delta}$ (of $x = 0$, 0.002, 0.008, 0.1, 0.20) measured at 700 °C. Data for $x = 0.1$ previously reported in Ref. 7.

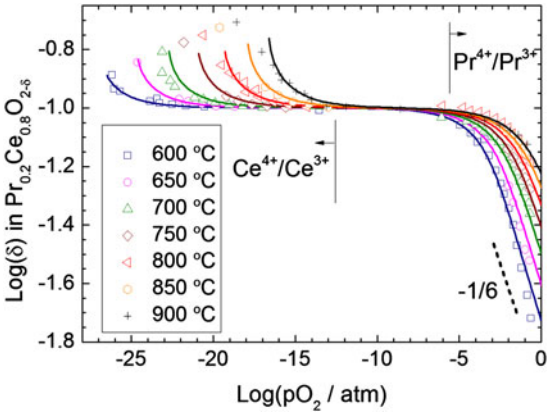


FIG. 2. Log δ plotted against log P_{O_2} for $Pr_{0.2}Ce_{0.8}O_{2-\delta}$ for a series of isotherms. The present defect model (solid lines) is fit to experimental data (points) from Ref. 17.

IV. RESULTS

The oxygen partial pressure dependence of the electrical conductivity, measured at 700 °C, is plotted in Fig. 1 as a function of Pr content, x in $Pr_xCe_{1-x}O_{2-\delta}$. Starting from highly reducing conditions, as P_{O_2} is increased, all compositions show a decrease in conductivity, reaching a plateau, followed by either an increase ($x = 0.2$), a further decrease in conductivity ($0 < x < 0.2$), or nominally no change ($x = 0$). The plateau in conductivity correlates with a plateau in oxygen stoichiometry as seen, e.g., in Fig. 2 (for $x = 0.2$), with δ increasing as P_{O_2} is reduced and decreasing as P_{O_2} is increased at the two extremes of the plateau, respectively.

The low P_{O_2} conductivity dependence arises from the reduction of cerium with the consequent generation of additional oxygen vacancies (as observed in Fig. 2) along with electrons (small polarons) consistent with the defect reaction given in Eq. (1) and with charge neutrality, Eq. (6), simplified as $n \approx 2[V_O^{\bullet\bullet}]$.[3,4] This, in turn, leads to mixed ionic electronic conductivity. In the intermediate P_{O_2} region, where the conductivity exhibits a plateau, cerium remains largely as Ce^{4+}, while Pr is fully reduced to Pr^{3+}, thereby acting as an acceptor dopant with Eq. (6) simplified as $[Pr_{Ce}'] \approx 2[V_O^{\bullet\bullet}]$. Similarly, background impurities, with 3+ or 2+ valence, fix the oxygen vacancy concentration for nominally undoped ceria.[3] In this ionic plateau region, therefore, the activation energy for electrical conduction is characterized solely by the oxygen ion migration energy [see Eqs. (10) and (11)].

At high P_{O_2}, Pr^{3+} oxidizes to Pr^{4+}, resulting in (i) a decrease in the oxygen vacancy concentration, and hence ionic conductivity, and, (ii) only at large enough Pr concentrations, an electronic contribution from electron hopping between Pr ions having formed an impurity band.

The concentration of oxygen vacancies was modeled using thermogravimetrically derived data (for $x = 0.2$[17] and 0.1[7]) by numerically solving Eqs. (1), (2), (4), and (6)–(9) as discussed previously in Ref. 7, with fitting to the data performed first visually and then refined with a least

https://doi.org/10.1557/jmr.2012.130 Published online by Cambridge University Press

squares-based analysis. H_r and K_r° were obtained from the low P_{O_2} region (i.e., Ce^{4+}/Ce^{3+} redox), and H_{Pr} and K_{Pr}° were obtained from the high P_{O_2} region (i.e., Pr^{4+}/Pr^{3+} redox) with the dependence of H_r on defect concentration, f, also derived and reported in Table II. The results of the fitting procedure are shown in Fig. 2 for $x = 0.2$, while those for $x = 0.1$ were presented previously in Ref. 7. At the lowest P_{O_2}, the model deviates positively from the data, as previously observed for the ceria system, and is believed to be associated with defect ordering.[18]

As discussed above, the plateau region at intermediate P_{O_2} is predominantly ionic and characterized by the activation energy for oxygen vacancy mobility, $H_{m,V}$. These data are plotted as log σT versus T^{-1} in Fig. 3 as a function of x in $Pr_xCe_{1-x}O_{2-\delta}$, with values of $H_{m,V}$ extracted from these Arrhenius plots reported in Table II. Next, $H_{m,e}$ and μ_e° in the low P_{O_2} region, μ_V° in the intermediate P_{O_2} region, and $H_{m,Pr}$ and μ_{Pr}° in the high P_{O_2} region were derived by fitting the conductivity model to the data [Eqs. (10)–(12)], using defect concentrations obtained from the previously derived defect equilibrium model. The resulting fits to conductivity data are shown in Figs. 4 and 5 for $x = 0.2$ and 0.1, respectively, with values for the parameters reported in Table II.

For the cases of $x = 0$, 0.008, and 0.002, there are no oxygen nonstoichiometry data available, requiring estimation of the thermodynamic parameters from conductivity measurements alone. Small polaron mobility via the Ce 4f band is reported not to be highly sensitive to either x or δ,[4,9] so $H_{m,e}$ and μ_e° were taken as the average of their respective values for $x = 0.2$ and 0.1. It was found that σ was mostly insensitive to f, except at low P_{O_2} and high T (i.e., high δ) with an estimate of $f = 2$ found to yield good fits in these regions. Additionally, the conductivity model was simplified by removing transport parameters associated with small polaron hopping on Pr ions since it was found that the conductivity for these compositions could be explained in the high P_{O_2} regime assuming only contributions from oxygen ion conductivity. Therefore, H_r and K_r° were obtained by fitting to the data in the low P_{O_2} region, μ_V° was obtained in the intermediate P_{O_2} region (using $H_{m,V}$ from Fig. 3), and H_{Pr} and K_{Pr}° were obtained from the high P_{O_2} region, with values reported in Table II. The results of the model fits are shown in Figs. 6 and 7.

For the case of nominally undoped ceria (Fig. 8), only the Ce^{4+}/Ce^{3+} redox is considered, and since there is no intentionally added dopant, the conductivity is dominated by small polaron hopping on Ce ions (except at high P_{O_2} and low temperature as discussed later). Like in the previous case, $H_{m,e}$ and μ_e° were taken as the average of their respective values for $x = 0.2$ and 0.1, with $f = 2$ found to yield good fits in high δ regions, thus leaving only H_r and K_r° to be extracted from fitting the conductivity data at low to intermediate P_{O_2}. At high P_{O_2} and temperatures below 800 °C, the conductivity exhibits the aforementioned plateau, the origin of which is discussed later.

V. DISCUSSION

A. Ionic and mixed ionic electronic conductivity

The $Pr_xCe_{1-x}O_{2-\delta}$ solid solution system is similar to other acceptor-doped ceria systems such as gadolinium- or samarium-doped ceria in that there is a wide P_{O_2}-independent conductivity regime in which the oxygen vacancy concentration is fixed and equal to half the acceptor ion concentration (i.e., $[Pr'_{Ce}] \approx 2[V_O^{\bullet\bullet}]$). Since the conductivity in this regime is predominantly ionic, and the carrier density is known, it is possible to readily calculate the oxygen vacancy mobility and migration energy as discussed above in relation to Fig. 3 and Table II.

An important figure of merit for such solid electrolytes is the maximum ionic conductivity achievable at a given temperature. The ionic conductivity at 800 °C of $Pr_xCe_{1-x}O_{2-x/2}$ (where all Pr is trivalent) is compared against that of $Gd_xCe_{1-x}O_{2-x/2}$, $Sm_xCe_{1-x}O_{2-x/2}$, and $Ca_xCe_{1-x}O_{2-x}$ as a function of dopant concentration in

TABLE II. Tabulation of the key thermodynamic and kinetic parameters defining defect generation and transport in $Pr_xCe_{1-x}O_{2-x/2}$ for studied values of x.

x in $Pr_xCe_{1-x}O_{2-\delta}$	0.2	0.1[a]	0.008	0.002	0
f, eV/δ	−3.02 ± 0.6	−4.63 ± 1.9	−2	−2	−2
H_r°, eV	3.99 ± 0.04	4.53 ± 0.04	4.96 ± 0.1	5.27 ± 0.1	5.18 ± 0.1
K_r°, $atm^{1/2}/cm^6$	(5.1 ± 2) × 10^{48}	(3.2 ± 1) × 10^{52}	(1.6 ± 0.2) × 10^{54}	(3.1 ± 0.3) × 10^{55}	(2.9 ± 0.4) × 10^{55}
H_{Pr}, eV	1.43 ± 0.03	1.43 ± 0.03	1.45 ± 0.08	1.63 ± 0.08	...
$K_{r,Pr}^\circ$, cm^3	(1.30 ± 0.3) × 10^{-23}	(8.18 ± 2) × 10^{-24}	(3.04 ± 1) × 10^{-24}	(4.07 ± 3) × 10^{-25}	...
$H_{m,V}$, eV	0.84 ± 0.06	0.70 ± 0.02	0.66 ± 0.02	0.75 ± 0.02	1.43 ± 0.06
μ_V°, cm^2 K/(V s)	250 ± 120	247 ± 40	262 ± 100	1516 ± 1000	...
$H_{m,Pr}$, eV	0.60 ± 0.04	0.56 ± 0.04	...	...	...
μ_{Pr}°, cm^2 K/(V s)	865 ± 300	801 ± 300	...	...	...
$H_{m,e}$, eV	0.38 ± 0.04	0.39 ± 0.1	0.39[b]	0.39[b]	0.39[b]
μ_e°, cm^2 K/(V s)	90 ± 60	127 ± 120	109[b]	109[b]	109[b]

[a]From Ref. 7.
[b]Average of values for $x = 0.2$ and 0.1.

https://doi.org/10.1557/jmr.2012.130 Published online by Cambridge University Press

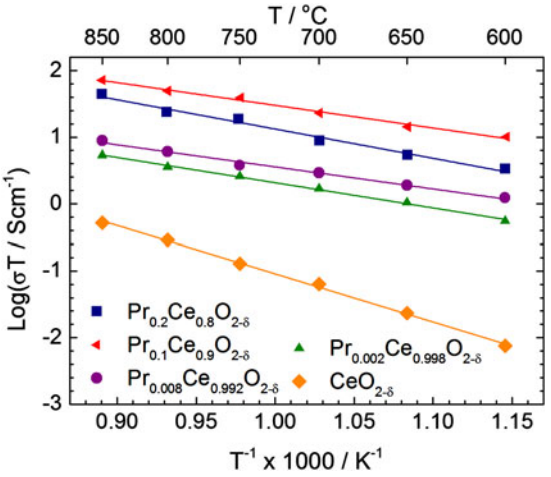


FIG. 3. The Ionic conductivity of $Pr_xCe_{1-x}O_{2-\delta}$ versus reciprocal temperature for different values of x obtained from the plateau region at intermediate P_{O_2}.

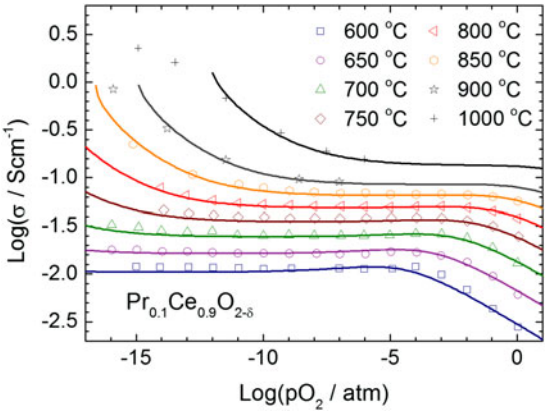


FIG. 5. Experimental electrical conductivity data (points) for $Pr_{0.1}Ce_{0.9}O_{2-\delta}$ are reported for a series of isotherms from 600 to 1000 °C. Solid lines represent predictions of the model derived in this study. Data and modeled values for 600–900 °C previously reported in Ref. 7.

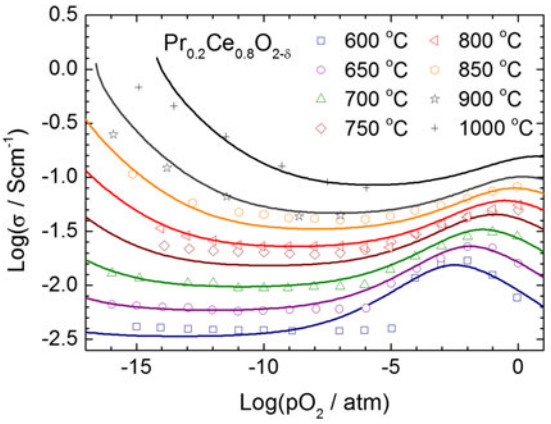


FIG. 4. Experimental electrical conductivity data (points) for $Pr_{0.2}Ce_{0.8}O_{2-\delta}$ are reported for a series of isotherms from 600 to 1000 °C. Solid lines represent predictions of the model derived in this study.

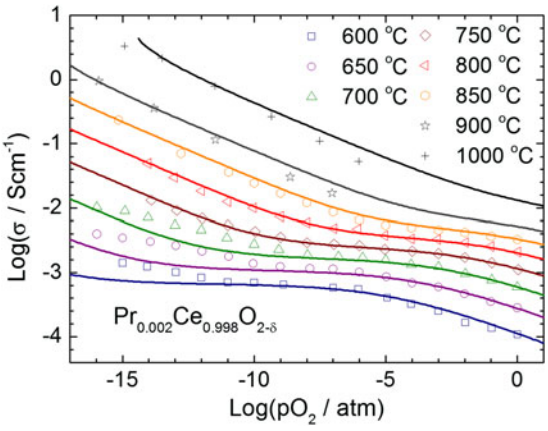


FIG. 6. Experimental electrical conductivity data (points) for $Pr_{0.008}Ce_{0.992}O_{2-\delta}$ are reported for a series of isotherms from 600 to 1000 °C. Solid lines represent predictions of the model derived in this study.

Fig. 9. $Gd_xCe_{1-x}O_{2-x/2}$ and $Sm_xCe_{1-x}O_{2-x/2}$ are typically used as ceria-based solid electrolytes in SOFCs since they have high ionic conductivities (nearly 0.1 S/cm at 800 °C). $Pr_xCe_{1-x}O_{2-x/2}$ exhibits similar values of ionic conductivity to those of the other trivalent-doped ceria up to $x = 0.1$ (i.e., 5×10^{-2} versus 5.5×10^{-2} and 7×10^{-2} S/cm for $Gd_xCe_{1-x}O_{2-x/2}$ and $Sm_xCe_{1-x}O_{2-x/2}$, respectively), with similar minimum $H_{m,V}$ values of ~0.7 eV.[19,20] However, while the latter two materials reach their peak conductivities at $\sim x = 0.2$, the Pr-doped system peaks earlier at $\sim x = 0.1$. Nevertheless, $Pr_xCe_{1-x}O_{2-x/2}$ with $x = 0.1$ and 0.2 still has ionic conductivities of approximately ½ or ¼ of that of the most highly conducting ceria-based electrolytes.

One may ask why the maximum for the Pr (as well as Ca)-doped ceria falls at a lower dopant concentration than that of Gd- or Sm-doped ceria. Both experimental and simulation studies have found for ceria that optimum ionic conductivities are achieved with dopant ions with radii and valence close to that of the host Ce ion. Defect–vacancy interactions become more evident for dopants with radii larger or smaller than the host cation radius, leading to reduced conductivity.[21–24] Note that while the ionic radius of Pr^{4+}, $r_{Pr^{4+}}$, is very close in size to $r_{Ce^{4+}}$ (0.97 Å), $r_{Pr^{3+}}$ (1.126 Å) is about 16% larger than $r_{Ce^{4+}}$, which could explain the shift in peak conductivity to lower dopant levels for the Pr-doped system.[25] This is also consistent with the increase in $H_{m,V}$ from 0.70 to 0.84 eV (see Fig. 10 and Table II) as one increases x in $Pr_xCe_{1-x}O_{2-x/2}$ from 0.1 to 0.2.

The very high oxygen ionic conductivity of $Pr_xCe_{1-x}O_{2-x/2}$ with $x = 0.1$ and 0.2 is a feature, which becomes particularly important given that both compositions also simultaneously exhibit comparably high

https://doi.org/10.1557/jmr.2012.130 Published online by Cambridge University Press

electronic conduction at high P_{O_2} as a consequence of electron hopping within the Pr-defect band. This then leads to mixed ionic electronic conduction in a ceria-based material under SOFC cathode conditions (e.g., air). This is illustrated in Fig. 11 in which the ionic transference number ($t_{ion} = \sigma_{ion}/\sigma_{total}$) of the four $Pr_xCe_{1-x}O_{2-\delta}$ solid solutions examined in this study are plotted as a function of log P_{O_2} for the temperature of 700 °C. As expected, the solid solutions containing low Pr fraction ($x = 0.002$ and 0.008) are fully ionic above log $P_{O_2} \sim 10^{-5}$ atm, while those with $x = 0.10$ and 0.20 show levels of electronic conductivity comparable to the ionic conductivity over this P_{O_2} range. Such mixed ionic electronic conductivity in a ceria material under oxidizing conditions would be expected to render it a good SOFC cathode material candidate. Indeed, the authors demonstrate in a recent publication that thin films of $Pr_xCe_{1-x}O_{2-\delta}$ with $x = 0.1$ and 0.2 exhibit cathode performance, with respect to oxygen exchange kinetics, comparable to perovskites such as (La,Sr)(Co,Fe)O_3, well known in the SOFC literature for superior performance at reduced temperatures.[10]

Turning briefly to the low temperature and high pO_2 region of conductivity in undoped ceria, and assuming that in this region, background acceptor impurities lead to ionic conduction, $H_{m,V}$ was extracted and is much larger than that for Pr or other acceptor-doped ceria. However, an alternative explanation for the high activation energy obtained in the high pO_2 σ plateau region of undoped ceria has been proposed.[26,27] These authors suggest that intrinsic electron–hole generation may be the source of this pO_2-independent conductivity. In this scenario, the activation energy corresponding to the slope in Fig. 3 for undoped ceria ($E_a = 1.43$ eV) would be given by the following equation.

$$E_a = \frac{E_g}{2} - H_{m,e} \quad , \tag{13}$$

where E_g is the energy gap between the Ce 4f and O 2p levels, and assuming electron mobility is much greater than hole mobility as found in Ref. 26. By this method, $E_g = 2.08$ eV is significantly less than that derived in previous studies (2.6–3.2 eV).[26,27] However, using this value to calculate intrinsic electron conductivity (using transport parameters in Table II and a density of states equal to the concentration of Ce),[3] one obtains an intrinsic conductivity of electrons at 700 °C equal to 2×10^{-5} S/cm, similar to that found in the high pO_2 region of Fig. 8 (7×10^{-5} S/cm).

B. Defect generation and nonstoichiometry

While acceptor-doped ceria exhibits the highest oxide ion conductivities for fluorite-structured oxides, it exhibits limited application in SOFCs due to its tendency to reduce under anodic fuel cell conditions, resulting in the generation of electronic carriers accompanied by partial short circuiting of the cell. According to Eq. (1), the reduction enthalpy, H_r, is the key parameter, which determines how readily ceria will reduce for a given temperature and P_{O_2}. It is therefore of interest to understand how H_r will depend on the type and concentration of acceptor dopants.

Examination of Fig. 10 and Table II shows that H_r tends to decrease from values above 5 eV at small x to 4.53 at $x = 0.1$ and finally down to 3.99 eV at $x = 0.2$. This demonstrates that increasing substitution of Pr^{3+} for Ce^{4+} combined with increasing levels of oxygen vacancies reduces the energy necessary to generate additional

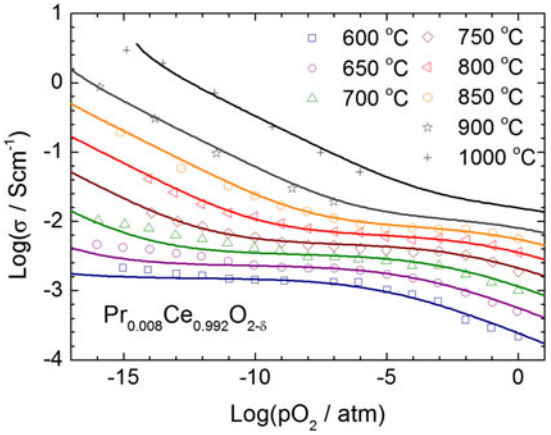


FIG. 7. Experimental electrical conductivity data (points) for $Pr_{0.002}Ce_{0.998}O_{2-\delta}$ are reported for a series of isotherms from 600 to 1000 °C. Solid lines represent predictions of the model derived in this study.

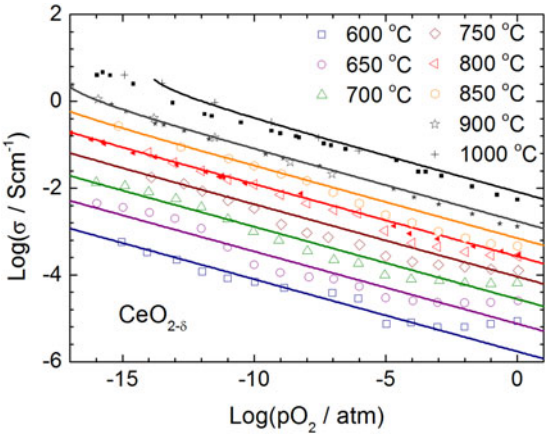


FIG. 8. Experimental electrical conductivity data (points) for nominally undoped $CeO_{2-\delta}$ are reported for a series of isotherms from 600 to 1000 °C. Solid lines represent predictions of the model derived in this study. Solid points (800, 900, and 1000 °C) represent single crystal conductivity data from the literature.[3] Note acceptor-doped behavior at high P_{O_2} and temperatures below 800 °C due to background impurities.

https://doi.org/10.1557/jmr.2012.130 Published online by Cambridge University Press

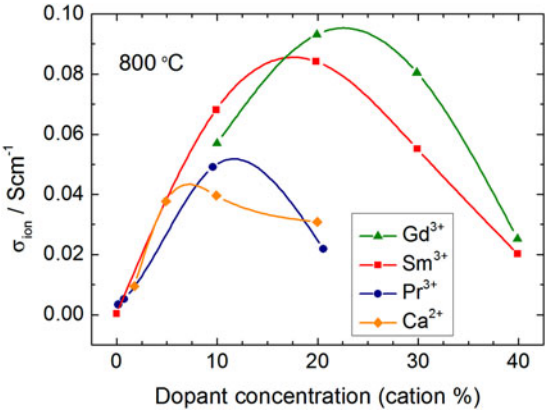


FIG. 9. The ionic conductivity measured at 800 °C as a function of acceptor dopant concentration for different ceria solid solutions from Refs. 28–30. For $Pr_xCe_{1-x}O_{2-x/2}$, all the Pr are in the trivalent state.

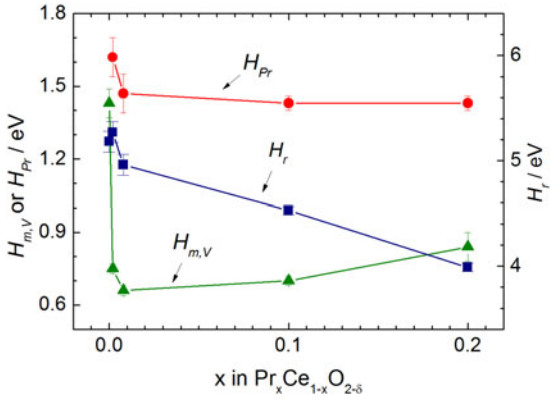


FIG. 10. Energies for defect formation or oxygen vacancy migration as a function of Pr content. (Note for $x = 0$, H_{Pr} is not calculated and $H_{m,V}$ is evaluated based on background acceptor impurities at high P_{O_2}, and H_r is reported for $\delta = 1/2[Pr]_{total}$.).

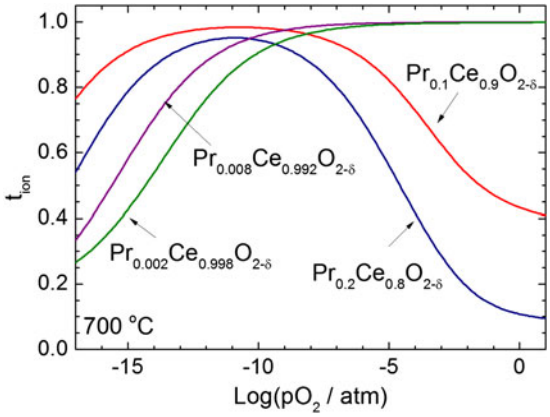


FIG. 11. Ionic transference number of $Pr_xCe_{1-x}O_{2-\delta}$ at 700 °C as a function of log P_{O_2} for designated values of x.

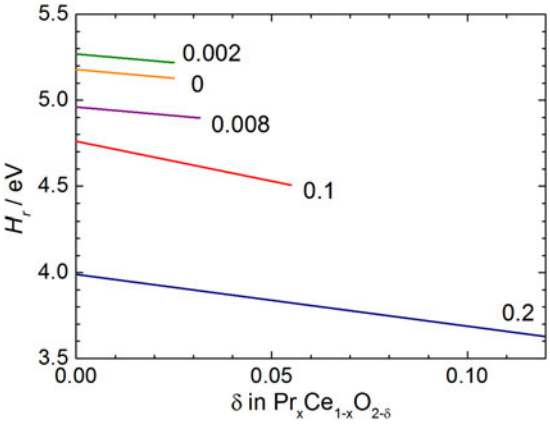


FIG. 12. Plot of ceria reduction enthalpy H_r as a function of oxygen nonstoichiometry for different levels of x, in accordance with Eq. (9). The range of plotted δ corresponds to the approximate range of δ in the conductivity measurements.

oxygen vacancies and Ce^{3+} ions. Accompanying the formation of oxygen vacancies is a *chemical expansion* arising primarily from the size difference of 3+ and 4+ valent cations, which, as the name implies, expands the lattice stretching bonds and likely plays a key role in reducing the binding energy of oxygen in the lattice.[12,13] Indeed, it has previously been observed that the elastic modulus, related to bond strength, decreases as the ceria lattice undergoes chemical expansion.[31] This is also consistent with the dependence of H_r on δ for a given value of x in $Pr_xCe_{1-x}O_{2-\delta}$ as reflected by Eq. (9) and shown in Fig. 12.

Next, we consider H_{Pr}, a measure of how far below the conduction band edge the Pr energy levels lie. H_{Pr} decreases from ~1.63 eV for very small x down to 1.43 eV for large x. Increasing levels of electronic conductivity at high P_{O_2} with increasing x is attributed, in this study, to the broadening of the Pr-derived impurity band. This would be consistent with a decrease in energy between the top of the Pr-derived impurity band and the bottom of the Ce 4f conduction band. A second contributor to this decrease in H_{Pr} could come from the fact that the band gap energy is correlated with bond strength, and according to the above discussion, increasing Pr could contribute to a reduced bond strength from chemical expansion. These suggested hypotheses need to be confirmed by further experimental and/or simulation studies.

VI. SUMMARY AND CONCLUSIONS

The thermodynamic transport and defect equilibria parameters of $Pr_xCe_{1-x}O_{2-\delta}$ as a function of x, from 0 to 0.2, were explored in this work. Trends with increasing x were observed, particularly in reduction enthalpies, H_r and H_{Pr}, consistent with a decrease in bond energy, potentially arising from chemical expansion, upon substitution of Ce^{4+} with Pr^{3+} and a widening of the Pr impurity band, respectively. $Pr_xCe_{1-x}O_{2-\delta}$ was found to exhibit high ionic conductivities, only somewhat lower than those of

https://doi.org/10.1557/jmr.2012.130 Published online by Cambridge University Press

Gd- and Sm-doped ceria. The peak in ionic conductivity occurred at somewhat lower substitution levels (e.g., $x = 0.1$ for Pr versus $x = 0.2$ for Gd and Sm) consistent with lattice distortions induced by the larger Pr^{3+} ion. The widening of the Pr levels into bands for $x \geq 0.1$ also results in mixed ionic electronic conductivity under typical SOFC cathode conditions. This creates options for utilizing acceptor-doped ceria not only as a solid electrolyte but also as a complementary cathode when appropriately doped.

ACKNOWLEDGMENTS

This research was funded by the Division of Materials Research, National Science Foundation under the Material World Network (DMR-0908627) in collaboration with Prof. Ralf Moos, Universität Bayreuth. S.R.B. recognizes partial support from I2CNER, supported by the World Premier International Research Center Initiative, MEXT, Japan. H.L.T. thanks I2CNER for hosting his visit during the time this manuscript was prepared. The authors wish to thank the reviewer for identifying potential intrinsic electronic conduction for undoped ceria in high pO_2.

REFERENCES

1. H. Inaba and H. Tagawa: Ceria-based solid electrolytes. *Solid State Ionics* **83**, 1–16 (1996).
2. B.C.H. Steele: Appraisal of $Ce_{1-y}Gd_yO_{2-y/2}$ electrolytes for IT-SOFC operation at 500 °C. *Solid State Ionics* **129**, 95–110 (2000).
3. H.L. Tuller and A.S. Nowick: Defect structure and electrical properties of nonstoichiometric CeO_2 single crystals. *J. Electrochem. Soc.* **126**, 209–217 (1979).
4. H.L. Tuller and A.S. Nowick: Small polaron electron transport in reduced CeO_2 single crystals. *J. Phys. Chem. Solids* **38**, 859–867 (1977).
5. S.B. Adler: Factors governing oxygen reduction in solid oxide fuel cell cathodes. *Chem. Rev.* **104**, 4791–4843 (2004).
6. C. Chatzichristodoulou, P.V. Hendriksen, and A. Hagen: Defect chemistry and thermomechanical properties of $Ce_{0.8}Pr_xTb_{0.2-x}O_2$. *J. Electrochem. Soc.* **157**, B299–B307 (2010).
7. S.R. Bishop, T.S. Stefanik, and H.L. Tuller: Electrical conductivity and defect equilibria of $Pr_{0.1}Ce_{0.9}O_{2-\delta}$. *Phys. Chem. Chem. Phys.* **13**, 10165–10173 (2011).
8. H.L. Tuller and S.R. Bishop: Point defects in oxides: Tailoring materials through defect engineering. *Annu. Rev. Mater. Res.* **41**, 369–398 (2011).
9. T.S. Stefanik and H.L. Tuller: Nonstoichiometry and defect chemistry in praseodymium-cerium oxide. *J. Electroceram.* **13**, 775–778 (2004).
10. D. Chen, S.R. Bishop, and H.L. Tuller: Praseodymium-cerium oxide thin film cathodes: Study of oxygen reduction reaction kinetics. *J. Electroceram.* **28**, 62–69 (2012) DOI: 10.1007/s10832-011-9678-z.
11. S.R. Bishop, J.J. Kim, N. Thompson, D. Chen, Y. Kuru, T. Stefanik, and H.L. Tuller: Mechanical, electrical, and optical properties of (Pr, Ce)O_2 solid solutions: Kinetic studies. *ECS Trans.* **35**, 1137–1144 (2011).
12. D. Marrocchelli, S.R. Bishop, H.L. Tuller, and B. Yildiz: Understanding chemical expansion in non-stoichiometric oxides: Ceria and zirconia case studies. *Adv. Funct. Mater.* DOI: 10.1002/adfm.201102648.
13. S.R. Bishop, H.L. Tuller, Y. Kuru, and B. Yildiz: Chemical expansion of nonstoichiometric $Pr_{0.1}Ce_{0.9}O_{2-\delta}$: Correlation with defect equilibrium model. *J. Eur. Ceram. Soc.* **31**, 2351–2356 (2011).
14. Y. Kuru, S.R. Bishop, J.J. Kim, B. Yildiz, and H.L. Tuller: Chemomechanical properties and microstructural stability of nanocrystalline Pr-doped ceria: An in situ x-ray diffraction investigation. *Solid State Ionics* **193**, 1–4 (2011).
15. T.S. Stefanik: Electrical properties and defect structures of praseodymium-cerium oxide solid solutions. Ph.D. Thesis, Massachusetts Institute of Technology, Cambridge, MA, 2004.
16. J. Van Herle, T. Horita, T. Kawada, N. Sakai, H. Yokokawa, and M. Dokiya: Low temperature fabrication of (Y, Gd, Sm)-doped ceria electrolyte. *Solid State Ionics* **86–88**, 1255–1258 (1996).
17. C. Chatzichristodoulou and P.V. Hendriksen: Oxygen nonstoichiometry and defect chemistry modeling of $Ce_{0.8}Pr_{0.2}O_{2-d}$. *J. Electrochem. Soc.* **157**, B481–B489 (2010).
18. S.R. Bishop, K.L. Duncan, and E.D. Wachsman: Surface and bulk oxygen non-stoichiometry and bulk chemical expansion in gadolinium-doped cerium oxide. *Acta Mater.* **57**, 3596–3605 (2009).
19. J. Faber, C. Geoffroy, A. Roux, A. Sylvestre, and P. Abelard: A systematic investigation of the dc electrical conductivity of rare earth doped ceria. *Appl. Phys. A* **49**, 225–232 (1989).
20. W. Lai and S.M. Haile: Impedance spectroscopy as a tool for chemical and electrochemical mixed conductors: A case study of ceria. *J. Am. Ceram. Soc.* **88**, 2979–2997 (2005).
21. R. Gerhardt-Anderson and A.S. Nowick: Ionic conductivity of CeO_2 with trivalent dopants of different ionic radii. *Solid State Ionics* **5**, 547–550 (1981).
22. V. Butler, C.R.A. Catlow, B.E.F. Fender, and J.H. Harding: Dopant ion radius and ionic conductivity in cerium dioxide. *Solid State Ionics* **8**, 109–113 (1983).
23. D.A. Andersson, S.I. Simak, N.V. Skorodumova, I.A. Abrikosov, and B. Johansson: Optimization of ionic conductivity in doped Ceria. *Proc. Natl. Acad. Sci. U.S.A.* **103**, 3518–3521 (2006).
24. J.A. Kilner and C.D. Waters: The effects of dopant cation oxygen vacancy complexes on the anion transport properties of non-stoichiometric fluorite oxides. *Solid State Ionics* **6**, 253–259 (1982).
25. R.D. Shannon: Revised effective ionic radii and systematic studies of interatomic distances in halides and chalcogenides. *Acta Crystallogr. Sect. A* **32**, 751–767 (1976).
26. M.A. Panhans and R.N. Blumenthal: A thermodynamic and electrical conductivity study of nonstoichiometric cerium oxide. *Solid State Ionics* **60**, 279–298 (1993).
27. Y-P. Xiong, H. Kishimoto, K. Yamaji, M. Yoshinaga, T. Horita, M.E. Brito, and H. Yokokawa: Electronic conductivity of pure ceria. *Solid State Ionics* **192**, 476–479 (2011).
28. H. Yahiro, Y. Eguchi, K. Eguchi, and H. Arai, Oxygen Ion Conductivity of the Ceria Samarium Oxide System with Fluorite Structure, *J. Appl. Electrochem.* **18**, 527–531 (1988).
29. T. Kudo and H. Obayashi, Mixed electrical conduction in the fluorite-type $Ce_{1-x}Gd_xO_{2-x/2}$, *J. Electrochem. Soc.* **123**, 415–419 (1975).
30. H. Yahiro, T. Ohuchi, K. Eguchi, and H. Arai, Electrical properties and microstructure in the system ceria alkaline-earth oxide, *J. Mater. Sci.* **23**, 1036–1041 (1988).
31. K. L. Duncan, Y. Wang, S. R. Bishop, F. Ebrahimi, and E. D. Wachsman: Role of point defects in the physical properties of fluorite oxides. *J. Am. Ceram. Soc.* **89**, 3162–3166 (2006).

https://doi.org/10.1557/jmr.2012.130 Published online by Cambridge University Press